Available online at www.sciencedirect.com
ScienceDirect
Trans. Nonferrous Met. Soc. China 34(2024) 2521−2532
Transactions of Nonferrous Metals Society of China
www.tnmsc.cn

Microstructural evolution and mechanical properties of duplex-phase Ti6242 alloy treated by laser shock peening

Pu-ying SHI[1,2], Xiang-hong LIU[2], Yong REN[2], Zeng TIAN[3], Feng-shou ZHANG[2], Wei-feng HE[1]

1. Institute of Aeronautics Engine, School of Mechanical Engineering, Xi'an Jiaotong University, Xi'an 710049, China;
2. Western Superconducting Technologies Co., Ltd., Xi'an 710018, China;
3. School of Aeronautical Engineering, Air Force Engineering University, Xi'an 710038, China

Received 12 January 2023; accepted 20 October 2023

Abstract: The effects of laser shock peening (LSP) on the microstructural evolution and mechanical properties of the Ti6242 alloy, including the residual stress, surface roughness, Vickers microhardness, tensile mechanical response, and high-cycle fatigue properties, were studied. The results showed that the LSP induced residual compressive stresses on the surface and near surface of the material. The maximum surface residual compressive stress was −661 MPa, and the compressive-stress-affected depth was greater than 1000 μm. The roughness and Vickers micro-hardness increased with the number of shocks, and the maximum hardness-affected depth was about 700 μm after three LSP treatments. LSP enhanced the fraction of low-angle grain boundaries, changed the grain preferred orientations, and notably increased the pole density of α phase on the near surface from 2.41 to 3.46. The surface hardness values of the LSP samples increased with the increase of the number of shocks due to work hardening, while the LSP had a limited effect on the tensile properties. The high-cycle fatigue life of the LSP-treated sample was significantly enhanced by more than 20% compared with that of the untreated sample, which was caused by the suppression of the initiation and propagation of fatigue cracks.

Key words: duplex-phase Ti6242 alloy; surface modification; laser shock peening; gradient microstructure; high-cycle fatigue properties

1 Introduction

The titanium alloy Ti6242, with the nominal composition of Ti−6Al−2Sn−4Zr−2Mo (wt.%, called TA19 in China), is a near α-type alloy. Owing to its high specific strength, excellent performance, and microstructural stability at high temperatures up to 500 °C [1−3], this alloy has been widely used for aircraft gas turbine components, afterburner structures, and hot sections in power generation [4−6]. Although the basic properties of the Ti6242 alloy satisfy the design requirements for these applications, recent studies have shown that some failure accidents, caused by fatigue fracture, still occur [7].

Previous studies [8−10] have indicated that the mechanical properties of this alloy are strongly influenced by its microstructure and the stress state of the component. Fatigue failure tends to take place unexpectedly under lower stresses with fewer service cycles [11−13], which brings great potential danger to the security of components and equipment. Residual compressive stresses in components are considered to be beneficial to their performance, especially for their high-cycle fatigue (HFC) properties [14−16]. Laser shock peening (LSP), as a promising material surface strengthening method, provides high-energy (GW/cm^2) laser pulses on the

Corresponding author: Wei-feng HE, Tel: +86-29-86514504, E-mail: spy@c-wst.com
DOI: 10.1016/S1003-6326(24)66557-X

material surface in a very short time (ns) and introduces compressive residual stresses on the surface [17−20].

LSP plays an important role in surface grain refining. The micro-scale sub-grains formed by LSP impede the motion of dislocations and the initiation of fatigue cracks, thus extending the fatigue life of a material [21,22]. Furthermore, the hardened layer generated by LSP improves the wear resistance and corrosion resistance of the material [23,24]. It has been found that the surface roughness characteristics of components are closely related to their fatigue lives, i.e., under the same loading condition, a higher roughness leads to a lower fatigue life. The laser shock leaves craters on the material surface and increases the surface roughness, so it is necessary to control the LSP parameters to avoid surface roughness-induced material performance degradation [25,26]. However, limited studies on the LSP effects on the microstructural evolution and mechanical properties of the Ti6242 alloy can be found in the existing literature [16,21].

In this work, LSP was performed for different time on the surface of the Ti6242 alloy with a dual-phase microstructure. The surface roughness, residual stresses, Vickers hardness, macro/microstructures, and tensile and high-cycle fatigue properties of the alloy were investigated, and finally, the fracture mechanisms of the LSP-treated Ti6242 alloys were also clarified.

2 Experimental

2.1 Materials

The as-received material was a forged Ti6242 bar with a diameter of 260 mm, manufactured by Western Superconducting Technologies Co., Ltd., China. The actual chemical compositions of the Ti6242 bar are listed in Table 1. The beta transformation temperature (T_β) of the Ti6242 alloy was measured to be 1010−1015 °C. The sample was subjected to a solution heat treatment of T_β−40 °C, and then it was aged at 595 °C for 8 h before use. After sufficient hot deformation and heat treatment in the α+β region, the Ti6242 alloy possessed a homogenous bimodal microstructure, which consisted of 30%−35% of the equiaxed primary α phase and transformed β matrix. An optical microscopy (OM) image showing the morphology of the Ti6242 alloy is shown in Fig. 1.

Table 1 Chemical composition of Ti6242 alloy (wt.%)

Al	Sn	Zr	Mo	Si
5.5−6.5	1.8−2.2	3.6−4.4	1.8−2.2	0.06−0.10
Fe	O	N	C	H
≤0.10	≤0.15	≤0.05	≤0.05	≤0.01
Y	Others, each	Others, total		Ti
≤0.005	≤0.1	≤0.3		Bal.

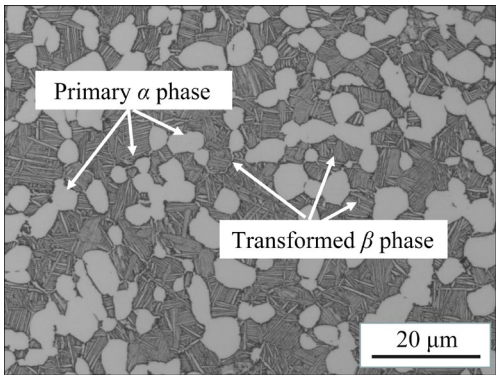

Fig. 1 OM image showing morphology of Ti6242 alloy

2.2 Experimental procedure

LSP experiments were performed using a YS100−R200A laser shock equipment from Xi'an Tianruida Optoelectronic Technology Co., Ltd., China. In the process of LSP, a neodymium-doped yttrium aluminum garnet (Nd:YAG) laser with a pulse of 20 ns and a wavelength of 1064 nm was applied. Single-channel laser shocks were applied on all samples with a laser energy of (7±0.2) J and a spot diameter of (2.6±0.1) mm. The overlap rate was 50%. The laser pulse width was 18−20 ns, A 1 mm-thick water layer was used as the transparent confining layer, and 100 μm-thick black tape was used as the absorbing layer to protect the specimen surface from thermal ablation.

Surface roughness was measured on the same sample used to measure the microhardness by using a WALE SP2102R roughness profile all-in-one system. Residual stresses were measured by the "cos α" method with the Pulstec u360 device on the clamping section of the broken tensile sample, which did not participate in deformation during stretching. Laser shocks were applied three times on the sample in the direction perpendicular to the test plane with a laser energy of 7 J. Surface residual stresses and residual stresses within the solid were measured at intervals of 100 μm, and the electrochemical stripping method was used for material removal.

Micro-hardness measurements were carried out using a Vickers indenter with a load of 200 g and a hold time of 30 s. The hardness on the surface and in the sub-surface was measured at intervals of 100 μm along the depth direction. The micro-structures were observed and analyzed by electron back-scattered diffraction (EBSD, JMS-IT700HR, Japan).

The specimens used for tensile and high-cycle fatigue tests were wire-electrode machined according to the drawing shown in Fig. 2, and the laser shocked areas are shown as shaded areas. Prior to the LSP treatment, the surfaces of all the specimens were polished with SiC paper with different roughness grades, followed by cleaning in deionized water. An MTS tensile testing machine was used to carry out tensile tests at room temperature and a speed of 0.015 mm/min. A QBG−100 high-frequency testing machine was used to carry out high-cycle fatigue tests. The stress amplitude was 450 MPa and the stress ratio R was −1. The tensile and fatigue fracture morphologies were observed by scanning electron microscopy (SEM, ZEISS).

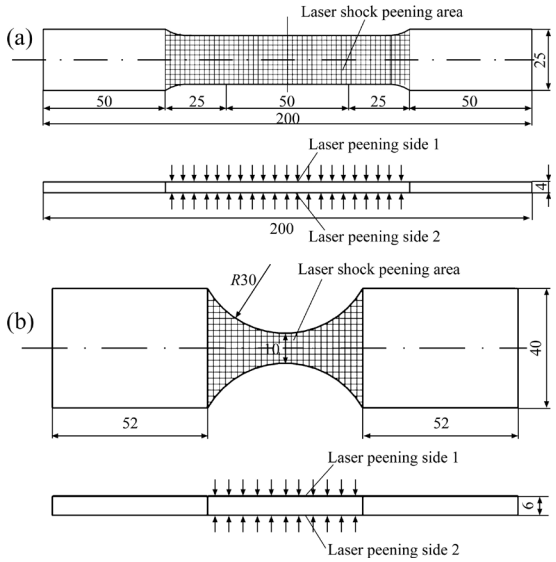

Fig. 2 Schematic diagrams of tensile (a) and high-cycle fatigue (b) test specimens (Unit: mm)

3 Results and discussion

3.1 Surface roughness

During laser shock processing, a high-energy laser was applied to the surface of the material, forming circular dents on the material surface with a Gaussian distribution of the laser spot energy. The dents were depressed in the center and bulged at the edges, creating peak–valley fluctuations at the macro-level on the shocked surface, resulting in an increased surface roughness. The surface profiles and surface roughness values of the Ti6242 alloys after one, three, and five LSP treatments are shown in Fig. 3, where 7J1 LSP, 7J3 JSP and 7J5 LSP represent samples undergoing laser shock peening with energy of 7 J and shock times of one, three and five, respectively. After one shock, arc-bottom impact dents were generated on the surface of a sample, the average height difference between the peaks and valleys was about 3 μm, and the average distance between the two peaks was approximately 1.4 mm, associated with a surface roughness (R_a) of ~0.423 μm, as shown in Fig. 3(a). After three shocks,

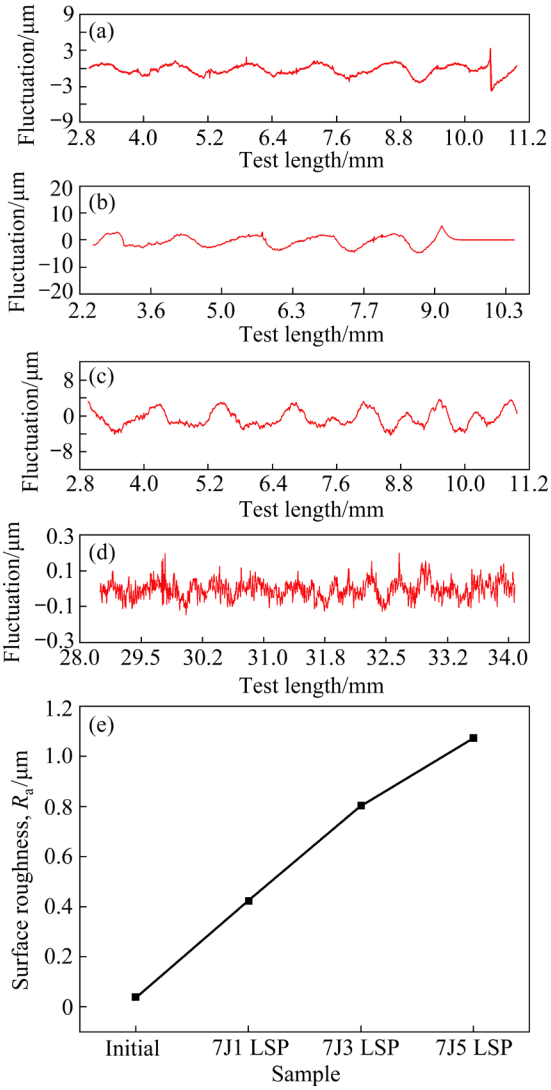

Fig. 3 Surface profiles and surface roughness of Ti6242 alloy with and without LSP: (a) One shock; (b) Three shocks; (c) Five shocks; (d) Initial surface without LSP; (e) Surface roughness comparison

the height difference increased to 7 μm, the distance was approximately 1.25 mm, and R_a was about 0.802 μm, as shown in Fig. 3(b). As the impact number increased to five, the height difference continued to increase to 8 μm, the distance between two peaks decreased to approximately 1.15 mm, and the roughness R_a was calculated to be 1.073 μm, as shown in Fig. 3(c). By contrast, the surface roughness of the Ti6242 alloy without LSP was measured to be 0.039 μm, as shown in Fig. 3(d). However, it was found that there were many micro-fluctuations on the surfaces of the laser shock-free samples, which were induced by sample machining. These may have been sources of cracks during service. The combination of the proper LSP parameters and the shock times resulted in a relatively flat dented bottom, which improved the surface integrity and reduced the stress concentration on the material surface. This would be beneficial to improving the fatigue performance. Figure 3(e) displays the surface roughness values of the LSP-treated and untreated specimens, revealing that the surface roughness of the material increased with the increase in the number of laser shocks.

3.2 Residual stress

The residual stresses were measured on the surface and in the depth direction. The appearances of the samples and residual stress test positions marked with red circles are shown in Fig. 4. Residual stresses in the x direction were measured, because it was the direction of the LSP.

Ten points were randomly selected for surface residual stress measurement, and the results are shown in Fig. 5(a). It can be seen that the surface residual stresses were negative, which meant that residual compressive stress existed on the surface of the material. The minimum residual compressive stress value was −357 MPa, while the maximum value was −661 MPa. The calculated coefficient of variation (CV, which is defined as the standard deviation divided by the mean) of the compressive stress reached 17%. This indicated that the surface residual compressive stress value had a certain

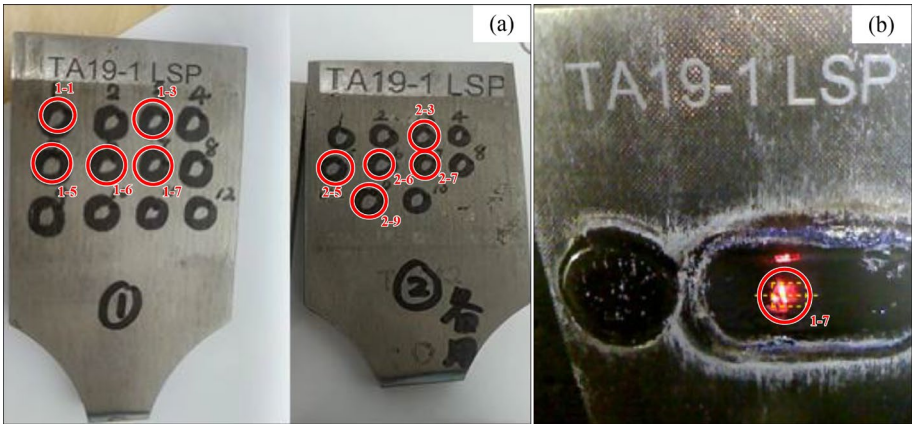

Fig. 4 Appearances of samples and residual stress test positions: (a) Surface; (b) Depth direction

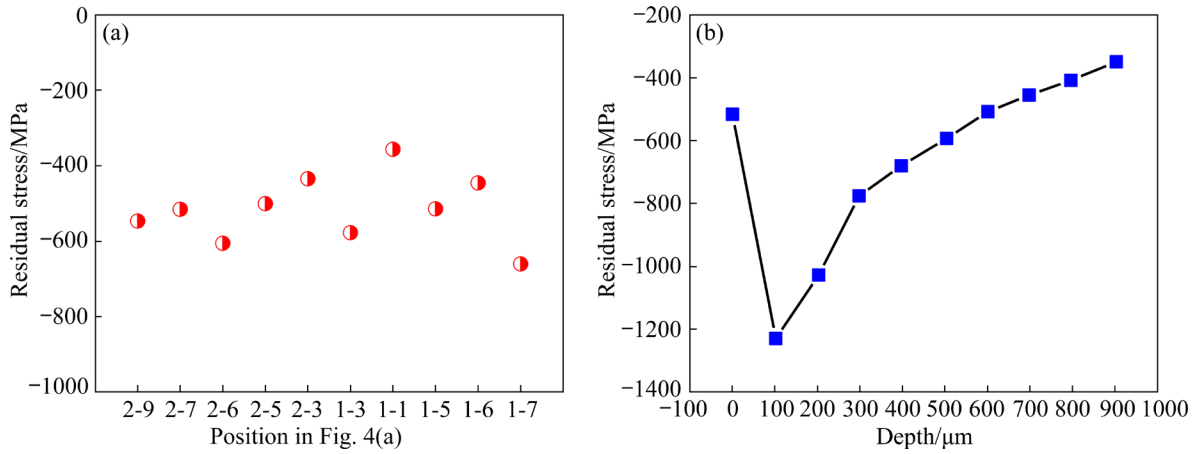

Fig. 5 Residual stress on surface (a) and in depth direction (b)

dispersion, that is to say, the residual compressive stress was unevenly distributed on the shock surface, even though the sample experienced three laser shocks with path overlaps of 50%. The residual stress in the depth direction was tested at intervals of 100 μm, as shown in Fig. 5(b). The residual stress in the depth direction was compressive stress, which decreased with the increase in the depth. The maximum compressive stress was −1230 MPa at a depth of 100 μm. In addition, the maximum compressive stress did not appear on the surface of the sample. When the depth reached 1000 μm, the residual stress was still negative, implying that the thickness of the compressive residual stress layer was larger than 1000 μm. The existence of this compressive stress layer was proven to be beneficial to the high-cycle fatigue performances of materials [17−22].

3.3 Microhardness

The microhardness was measured for the Ti6242 alloy on the LSP-treated surface and in the depth direction, as shown in Fig. 6. Compared with the initial material, the Vickers hardness of the LSP-treated sample increased as the number of shocks increased. To ensure the reliability of the results, surface hardness values were tested at five locations, as shown in Fig. 6(a). The Vickers hardness values of the alloy after one, three, and five LSP cycles were HV 368, HV 382 and HV 388, respectively, which were 19%, 23%, and 25% higher than that of the untreated material, respectively. In addition, when the number of shocks increased from three to five, the hardness value only increased by 2%, which was considered the saturation hardness on the surface [27,28]. Figure 6(b) shows the hardness distribution in the depth direction after three shocks. The hardness value displayed a decreasing tendency as the depth increased until 700 μm, and then the hardness was constant and approached that of the matrix. This meant that three LSP treatments created a 700 μm depth hardening layer on the surface of the Ti6242 alloy.

The above results indicate that the surface and near-surface microhardness values of the Ti6242 alloy could be effectively improved by LSP. More than one shock had a stronger effect on the surface and subsurface hardening. However, when the number of LSP processes was greater than three, the LSP did not significantly enhance the hardness of the Ti6242 alloy, but resulted in an increased surface roughness. Therefore, it is not suitable to use the LSP multiple times (more than three times) in engineering to enhance the hardness of the Ti6242 alloy.

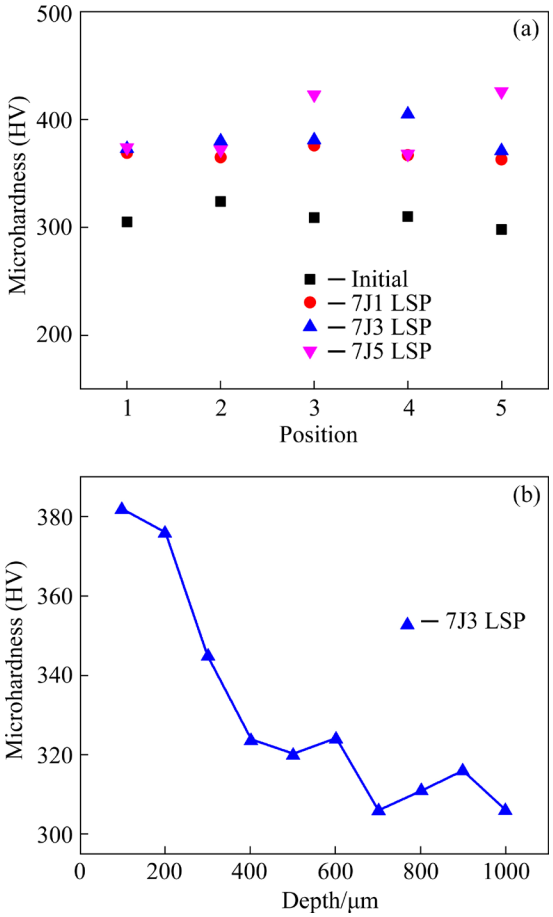

Fig. 6 Microhardness of Ti6242 alloy on surface (a) and in depth direction (b)

3.4 Microstructures

The surface and mechanical properties of metal materials are strongly related to their microstructural characteristics, such as their grain sizes, grain boundary characters, textures, and stress states. During the laser shock process, the shock-wave acts on the surface of the alloy, resulting in severe plastic deformation. Specifically, this process generates a large number of dislocations, which may evolve into dislocation entanglements and dislocation walls through multiplication, movement, and settlement, thus resulting in grain refinement [27]. At the same time, low-angle grain boundaries (LAGBs) may be induced by LSP, forming sub-crystals to refine the grains. In addition, LSP can reduce the textural strength, improving the deformation heterogeneities [29].

Two regions near the surface with dimensions of 1125 μm (depth) × 150 μm (width) and 150 μm (depth) × 200 μm (width) underwent three LSP treatments and were analyzed by EBSD. These areas, named Areas 1 and 2, respectively, are shown in Fig. 7(a). The inverse pole figure (IPF) maps of Areas 1 and 2 are shown in Figs. 7(b) and (c), respectively. From these maps, we can see that the grain size near the surface was smaller than that of the matrix, and severe plastic deformation occurred near the material surface. Figures 7(d) and (e) display the misorientation distribution frequencies of Areas 1 and 2, respectively. The fraction of LAGBs in Area 1 was approximately 28%, while for Area 2, it reached up to 53%, about twice that of Area 1. Furthermore, for the two other grain boundary mismatch peaks, at 60° and 90°, the frequencies for Area 1 were 4% and 4%, respectively, which were higher than the corresponding values of 2% and 2% for Area 2. These results indicated that a large number of LAGBs were produced by the LSP process, and the appearance of these LAGBs did not only provide the possibility for the grain refinement but also facilitate the surface hardness enhancement.

The pole figures of both the α and β phases of these two areas are displayed in Fig. 8. The preferred orientation of the α phase in Area 1 was [001] in the Z_0 direction, with the maximal pole density of 2.41, as shown in Fig. 8(a). By contrast, the preferred orientation of the α phase in Area 2 was [001] in the Y_0 direction, and the maximal pole density increased to 3.46, as shown in Fig. 8(b). The preferred orientation of the β phase was [101] in the Y_0 direction and between [101] and [111], with the maximal pole density of 3.31, as shown in Fig. 8(c). For the β phase, the preferred orientation changed from pole points to lines and arcs between the poles, and the maximal pole density value decreased to 1.94, as shown in Fig. 8(d). These results implied that the preferred orientations of both the α and β phases changed during the LSP process. The pole density of the α phase increased, while that of the β phase decreased, which would affect the coordination of these two phases during the deformation and eventually influenced the

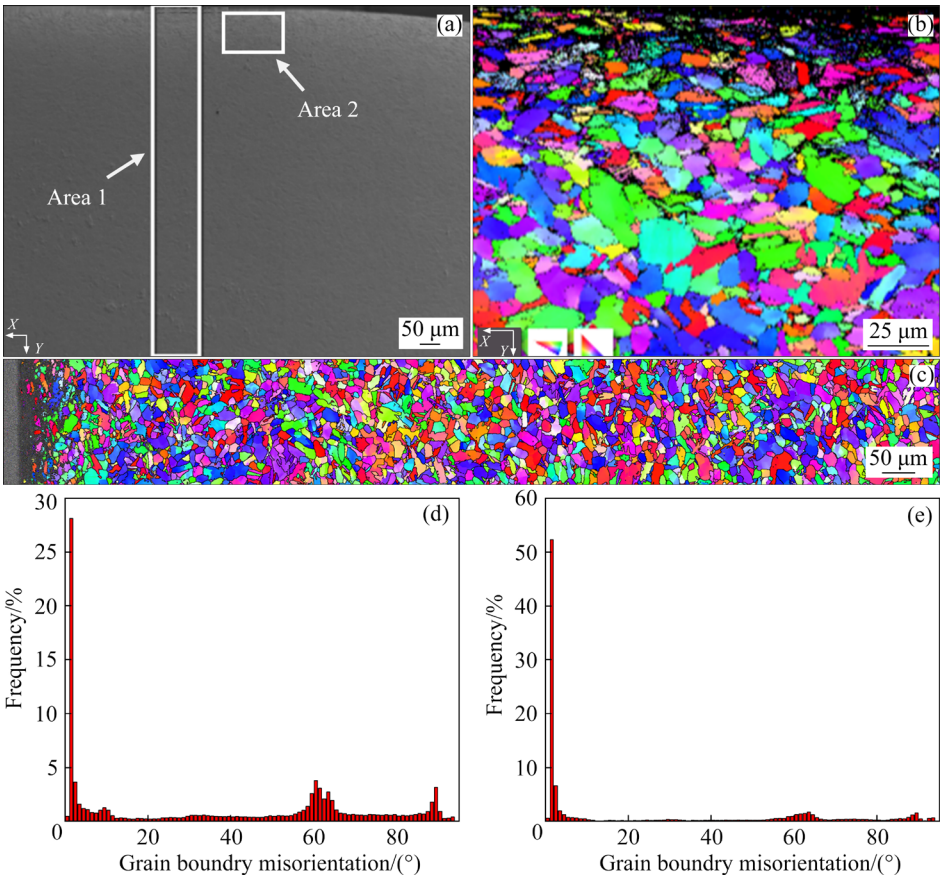

Fig. 7 Microstructural characterization of Ti6242 alloy after three LSP treatments: (a) Scanning areas; (b) IPF map of Area 1; (c) IPF map of Area 2; (d, e) Grain boundary (GB) misorientation distributions in Areas 1 (d) and 2 (e) in (a), respectively

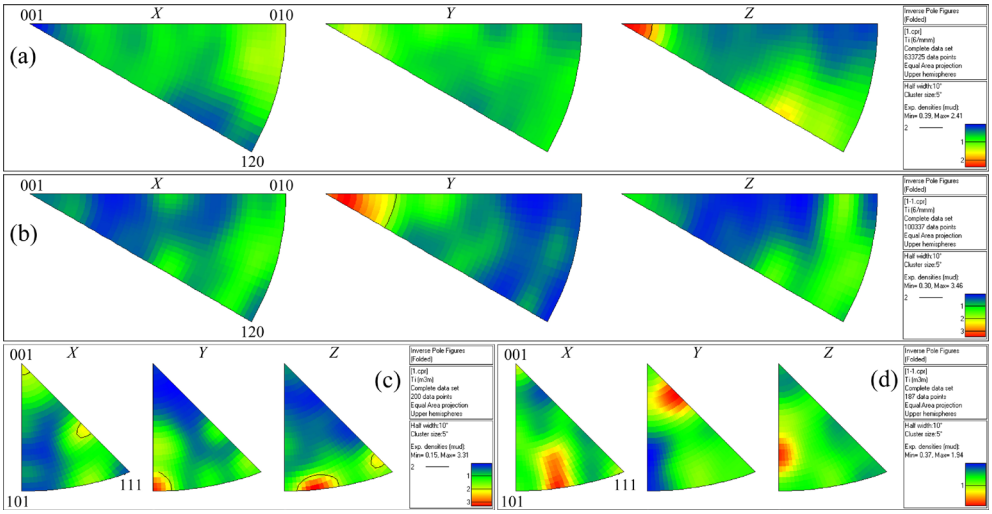

Fig. 8 Pole figures of Ti6242 alloy after three LSP treatments in two areas in Fig. 7(a): (a) α phase in Area 1; (b) α phase in Area 2; (c) β phase in Area 1; (d) β phase in Area 2

deformation behavior of the material. The Ti6242 alloy consisted of more than 90% α precipitates (about 35% of them were the primary α phase). The crystal structure symmetry of the hexagonal close-packed (HCP) α phase was lower than that of the body-centered cubic (BCC) β phase, which could easily form a texture during deformation in the Ti6242 alloys, and thus the reduced deformation coordination could lead to preferential cracking of the material. However, because the LSP reduced the forging texture of the β phase, the pole density of the β phase decreased after the LSP, which would be beneficial to the uniform deformation of the material under stress [29].

3.5 Mechanical properties

The Hall−Petch relationship summarizes the correlation between the yield strength of a material and the grain size, revealing that the yield strength is inversely proportional to the grain size. That is, smaller grains lead to a higher yield strength [30]. The results of the tensile mechanical properties of the LSP-treated and untreated specimens are shown in Fig. 9. We can see that the tensile strength of the LSP-treated specimen was 1112 MPa, somewhat higher than the value for the untreated specimen of 1102 MPa, while the yield strength of the LSP-treated specimen was slightly lower than that of the untreated specimen, as shown in Fig. 9(a). The LSP-treated specimens had more scattered yield strength values, and the CV value was calculated to be 2.2%. Meanwhile, the elongation of

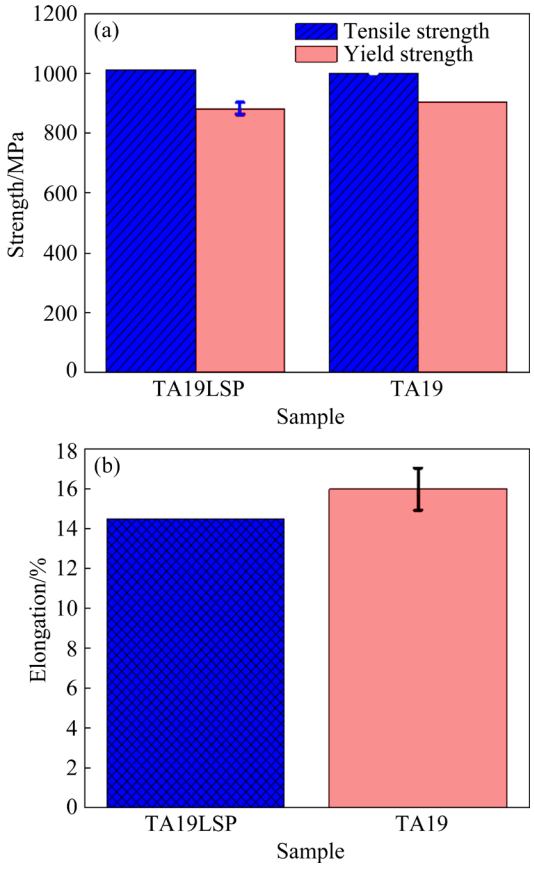

Fig. 9 Tensile properties of Ti6242 alloy with and without LSP: (a) Tensile strength and yield strength; (b) Elongation

the LSP sample was also slightly lower than that of the untreated specimen. The values were 14.5% and 16.0% for LSP-treated and untreated samples, respectively (Fig. 9(b)). The reductions in the yield strength and elongation were related to the decrease

in the α phase deformation coordination caused by the LSP. In general, laser shock strengthening had little effect on the macroscopic tensile properties of the Ti6242 alloy in this study.

The tensile fracture morphologies of the LSP-treated and untreated specimens were observed by SEM, and the results are shown in Fig. 10. It was found that the LSP-treated specimen had a compact surface with significant cleavage and inter-granular fracture characteristics. Dimples in the fracture were shallow and sparse, as shown in Figs. 10(a) and (c). However, for the untreated specimen, the fractures fluctuated significantly with dense and deep dimples, as shown in Figs. 10(b) and (d). The characteristics of the fracture surface were consistent with the material properties.

Fatigue testing was further carried out under load-controlled mode using sinusoidal cyclic loading, with a frequency of 100−120 Hz at room temperature. The stress amplitude was 450 MPa, and the stress ratio R was −1. The fatigue lives of the sample after three LSP treatments and the untreated specimen were 32922 and 27430 cycles, respectively. It was clear that the specimen with three LSP treatments had a longer fatigue life, about 20% higher than that of the untreated specimen. This was attributed to the compressive residual stress introduced by the LSP and the formation of fine crystals and sub-crystals in the surface layer, which strongly restricted the initiation and propagation of fatigue cracks [17,19].

Figure 11 displays the SEM images of the LSP-treated and untreated specimens after fatigue fracture. The fatigue fractures contained three regions for both the treated and untreated samples, namely a crack initiation region, a crack propagation region, and a fracture region, as shown in Figs. 11(a) and (b), respectively. However, the fractures had different features. The untreated sample had multi-source fatigue characteristics, i.e., crack initiation sites appeared on the upper and lower surfaces of the sample, and the fracture surface exhibited significant fluctuations, as shown in Fig. 11(a). The LSP-treated specimen had single-source fatigue characteristics, i.e., the crack initiation sites appeared on the side of the sample that was not enhanced by laser shock, and the fracture surface was relatively flat, as shown in Fig. 11(b). This meant that the LSP transferred the crack source from the strengthened surface to other weak sites. The enlarged image of the crack initiation site of the LSP-treated specimen is shown in Fig. 11(e). After initiation from the surface, the cracks propagated inward and formed fatigue striations in the direction perpendicular to that of the crack growth (see Fig. 11(c) for the untreated specimen and Fig. 11(f) for the LSP-treated specimen).

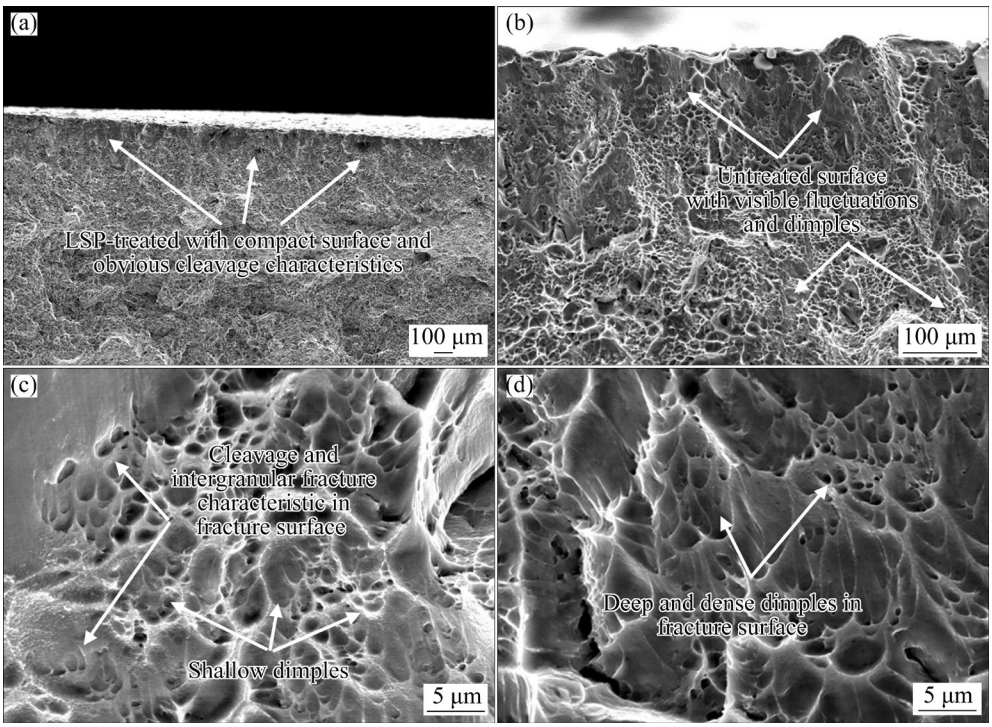

Fig. 10 Tensile fracture morphologies of LSP-treated (a, c) and untreated (b, d) specimens by SEM

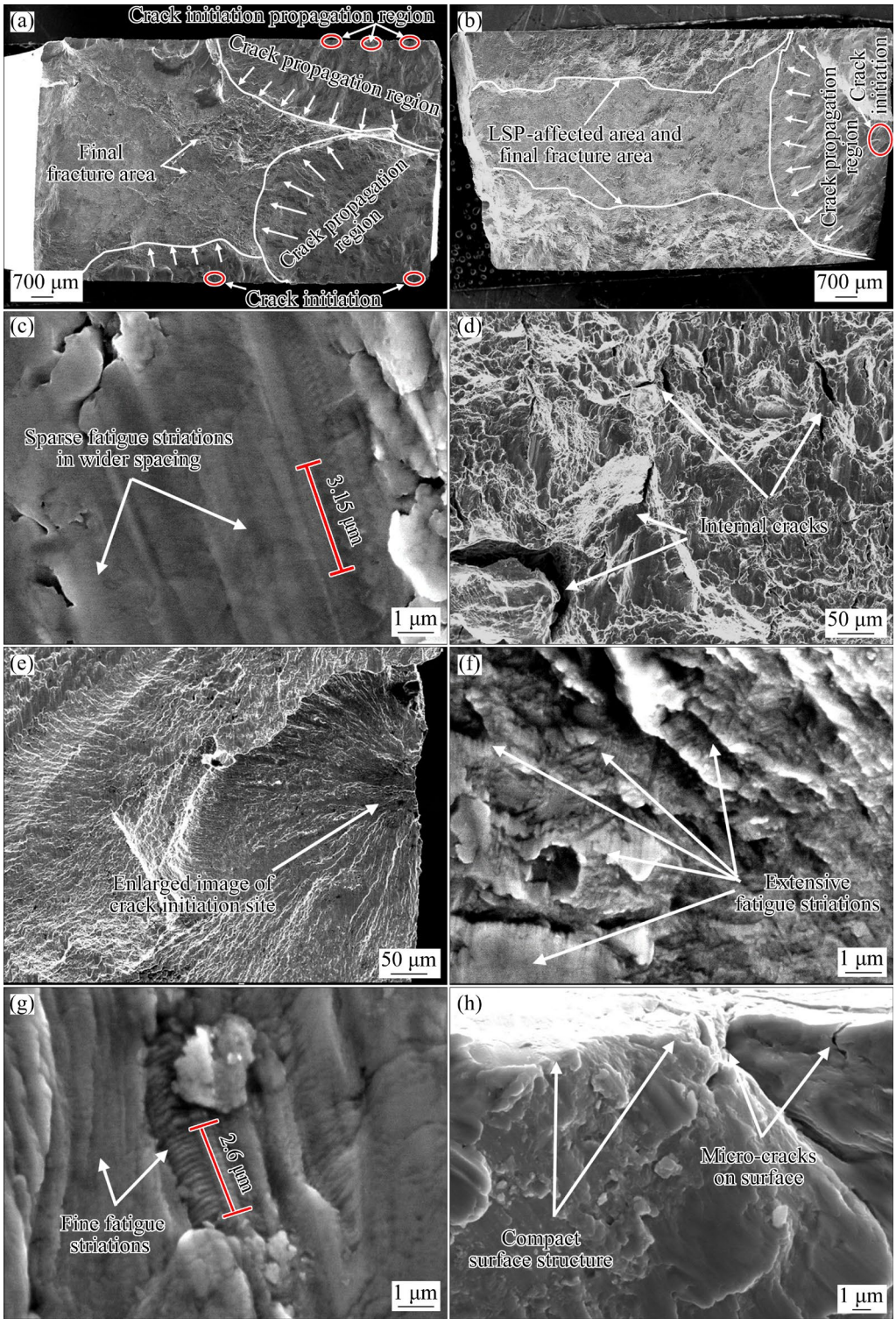

Fig. 11 SEM images of different specimes after high-cycle fatigue fractures: (a) Macro-fracture of untreated specimen; (b) Macro-fracture of LSP-treated specimen; (c, d) Microstructure of untreated fracture surface; (e–h) Microstructure of LSP-treated fracture surface

The fatigue striation spacing was determined to be 0.42 μm/cycle for the untreated specimen, as shown in Fig. 11(c), and 0.20 μm/cycle for the LSP-treated specimen at the same location from the crack initiation sites, as shown in Fig. 11(g). The spacing between the fatigue striations represented the distance of crack growth per cycle. Therefore, the crack growth rate of the LSP-treated specimen

was slower than that of the untreated specimen. Moreover, the LSP-treated specimen had more fatigue striations than the untreated specimen (see Figs. 11(c) and (f), respectively). For the fracture region of the untreated specimen, a certain number of internal micro-cracks appeared close to the center of the sample, as shown in Fig. 11(d). However, the fracture region of the LSP-treated specimen was closer to the surface, and the surface had compact characteristics, as shown in Fig. 11(h), indicating that the surface of the sample was strengthened and fractured at the last stage of crack propagation.

4 Conclusions

(1) LSP induced residual compressive stresses on the surface and near-surface of the material. The maximum surface residual compressive stress was −661 MPa, which did not appear on the surface of the sample, and the compressive-stress-affected depth was larger than 1000 μm, which decreased with the increase in the depth. The roughness and Vickers microhardness of the Ti6242 alloys increased with the number of laser shocks, and the maximum hardness and affected depth were about 700 μm for the sample that underwent three LSP treatments.

(2) A large number of LAGBs were generated near the surface of the alloy during LSP processing. The LSP also changed the grain preferred orientation on the surface of the Ti6242 alloy and increased the pole density of the α phase from 2.41 to 3.46, forming a hardened layer near the surface to increase the hardness of the sample. In general, LSP had little effect on the tensile mechanical properties of the Ti6242 alloy.

(3) Laser shock strengthening had a strong effect on the fatigue properties of the Ti6242 alloy. The high-cycle fatigue life of the LSP-treated specimen was approximately 20% longer than that of the untreated specimen. The fatigue crack initiated on the surface of the sample that was not LSP-strengthened. The fatigue striation spacing was 0.20 μm/cycle for the LSP specimen and 0.42 μm/cycle for the untreated specimen. This was due to the residual compressive stress in the surface caused by the LSP, inhibiting the initiation and propagation of fatigue cracks.

CRediT authorship contribution statement

Pu-ying SHI: Conceptualization, Data curation, Formal analysis, Methodology, Validation, Visualization, Writing − Original draft, Review & editing; **Xiang-hong LIU, Yong REN, Zeng TIAN,** and **Feng-shou ZHANG:** Methodology; **Wei-feng HE:** Supervision, Review.

Declaration of competing interest

The authors declare that they have no known competing financial interests or personal relationships that could have appeared to influence the work reported in this paper.

Acknowledgments

Mr. Zi-jun REN at Instrumental Analysis Center of Xi'an Jiaotong University, China, is gratefully acknowledged for useful suggestions on microstructure analysis based on EBSD. This work was supported by the National Natural Science Foundation of China (No. 52205240).

References

[1] CHAMANFAR A, PASANG T, VENTURA A, MISIOLEK W Z. Mechanical properties and microstructure of laser welded Ti−6Al−2Sn−4Zr−2Mo (Ti6242) titanium alloy [J]. Materials Science and Engineering A, 2016, 663: 213−224.

[2] REZAEE M, ZAREI-HANZAKI A, GHAMBARI M, NEZHADFAR P D, GHASEMI E. Flow characterization of a duplex near α Ti6242 alloy through interrelation of microstructural evolution, 3D activation energy map, and processing map [J]. Advanced Engineering Materials, 2016, 18 (6): 1075−1085.

[3] BOYER R R. An overview on the use of titanium in the aerospace industry [J]. Materials Science and Engineering A, 1996, 213: 103−114.

[4] BANERJEE D, WILLIAMS J C. Perspectives on titanium science and technology [J]. Acta Materialia, 2013, 61: 844−879.

[5] CHRISTIAN F R, PFEIFER T, JÖRG T, KREMMER T, BRABETZ M, CLEMENS H, MAYER S. Selective laser melting of a near-α Ti6242S alloy for high-performance automotive parts [J]. Advanced Engineering Materials, 2021, 23(12): 2001194.

[6] HAN Xiu-feng, WANG Lun, ZHU Ming-liang, LIAO Zhong-xiang, ZHANG Lu. Microstructures and mechanical properties research of electron beam welding joint of Ti6242 titanium alloy [J]. Chinese Journal of Rare Metals, 2021, 45(7): 778−785. (in Chinese)

[7] ZHANG Ming-da, CAO Jing-xia, LI Ting, ZHAI Zhan-jiang, SUI Nan, JIA Rong-guang, HUANG Xu. The effect of transformed β-phase on local area plastic deformation and dislocation characteristics of Ti6242s alloy under low-cycle fatigue and dwell fatigue [J]. Materials Science and

Engineering A, 2021, 802: 140643.

[8] LUO Hang, XU Ping-wei, LIN Ting-yi, ZHOU Lei, LUO Ming-lang, JIANG Zi-hao, LIANG Yi-long, LIANG Yu. Effect of $\alpha p/\beta$-trans interfacial microstructure on tensile property and deformation behavior in Ti6242 alloys [J]. Materials Science and Engineering A, 2022, 844: 143−149.

[9] RAVINDRANADH B, VEMURI M. Flow and fracture characteristics of near alpha titanium alloy [J]. Journal of Alloys and Compounds, 2016, 684: 162−170.

[10] CAO Zi-wen, ZHANG Jie, CHE Zhi-gang, ZOU Shi-kun. Residual stresses of compound strengthening case on TC17 titanium alloy by laser peening and shot peening [J]. Surface Technology, 2018, 47(11): 80−84.

[11] VERDHAN N, BHENDE D D, KAPOOR R, CHAKRAVARTTY J K. Effect of microstructure on the fatigue crack growth behaviour of a near-α Ti alloy [J]. International Journal of Fatigue, 2015, 74: 46−54.

[12] XIONG Y, KARAMCHED P S, NGUYEN C T, COLLINS D M, MAGAZZENI C M, TARLETON E, WILKINSON A J. Macroscopic analysis of time dependent plasticity in Ti alloys [J]. Journal of Materials Science & Technology, 2022, 124(29): 135−140.

[13] REZAEE M, ZAREI-HANZAKI A, MOHAMADIZADEHET A, GHASEMI E. High-temperature flow characterization and microstructural evolution of Ti6242 alloy: Yield drop phenomenon [J]. Materials Science and Engineering A, 2016, 673: 346−354.

[14] SOYAMA H, KORSUNSKY A M. A critical comparative review of cavitation peening and other surface peening methods [J]. Journal of Materials Processing Technology, 2022, 305: 117586.

[15] MENG Xian-kai, ZHOU Jian-zhong, SU Chun, HUANG Shu, LUO Kai-yu, SHENG Jie, TAN Wen-sheng. Residual stress relaxation and its effects on the fatigue properties of Ti_6Al_4V alloy strengthened by warm laser peening [J]. Materials Science and Engineering A, 2017, 680: 297−304.

[16] GUJBA A K, MAEDRAJ M. Laser peening process and its impact on materials properties in comparison with shot peening and ultrasonic impact peening [J]. Materials, 2014, 7(12): 7925−7974.

[17] CLAUER A H. Laser shock peening, the path to production [J]. Metals, 2019, 9(6): 626−626.

[18] SUNDAR R, GANESH P, GUPTA R K, RAGVENDRA G, PANT B K, KAIN V, RANGANATHAN K, KAUL R, BINDRA K S. Laser shock peening and its applications: A review [J]. Lasers in Manufacturing and Materials Processing, 2019, 6(4): 424−463.

[19] ZHANG Chao-yi, DONG Ya-lin, YE Chang. Recent developments and novel applications of laser shock peening: A review [J]. Advanced Engineering Materials, 2021, 23(7): 1−24.

[20] WU Jia-jun, ZHAO Ji-bin, QIAO Hong-chao, HU Xian-liang, YANG Yu-qi. Research on the technical principle and typical applications of laser shock processing [J]. Materials Today: Proceedings, 2021, 44(1): 722−731.

[21] CHEN Lan, REN Xu-dong, ZHOU Wang-fan, TONG Zhao-peng, SAMUEL A G, YE Yun-xia, REN Yun-peng. Evolution of microstructure and grain refinement mechanism of pure nickel induced by laser shock peening [J]. Materials Science and Engineering A, 2018, 728: 20−29.

[22] LUO Si-hai, HE Wei-feng, ZHOU Liu-cheng, NIE Xiang-fan, LI Ying-hong. Aluminizing mechanism on a nickel-based alloy with surface nanostructure produced by laser shock peening and its effect on fatigue strength [J]. Surface and Coatings Technology, 2018, 342: 29−36.

[23] NING Cheng-yi, ZHANG Guang-yi, YANG Ya-peng, ZHANG Wen-wu. Effect of laser shock peening on electrochemical corrosion resistance of IN718 superalloy [J]. Applied Optics, 2018, 57(10): 2467−2473.

[24] TONG Zhao-peng, REN Xu-dong, REN Yun-peng, DAI Feng-ze, YE Yun-xia, ZHOU Wang-fan, CHEN Lan, Ye Zhao. Effect of laser shock peening on microstructure and hot corrosion of TC11 alloy [J]. Surface and Coatings Technology, 2018, 335: 32−40.

[25] ZHANG Dong-chu, PEI Xu-ming. Effects of machining processes on surface roughness and fatigue life [J]. Chinese Journal of Mechanical Engineering, 2003, 15(16): 1374−1377. (in Chinese)

[26] LONG Bo, SU Lei, JIN Peng, XIAO Jiu-lin. Influence on fatigue life of compressor disk by surface roughness [J]. Aviation Maintenance & Engineering, 2017(4): 52−55.

[27] CHATTOPADHYAY A, MUVVALA G, SARKAR S, RACHERLA V, NATH A K. Effect of laser shock peening on microstructural, mechanical and corrosion properties of laser beam welded commercially pure titanium [J]. Optics & Laser Technology, 2021, 133: 106527.

[28] SHIGANOV I N, MISUROV A I, MELNIKOV D M. Laser shock peening of welded joints [J]. IOP Conference Series: Journal of Physics: Conference Series, 2018, 1109: 012018.

[29] LV Ji-ming, LUO Kai-yu, LU Hai-fei, WANG Zhao, LIU Jia-jun, LU Jin-zhong. Achieving high strength and ductility in selective laser melting Ti−6Al−4V alloy by laser shock peening [J]. Journal of Alloys and Compounds, 2022, 899: 163335.

[30] LIU Hui-xia, HU Yang, WANG Xiao, SHEN Zong-bao, LI Pin, GU Chun-xing, LIU Hong, DU Dao-zhong, GUO Chao. Grain refinement progress of pure titanium during laser shock forming (LSF) and mechanical property characterizations with nanoindentation [J]. Materials Science and Engineering A, 2013, 564: 13−21.

激光冲击强化双相 Ti6242 合金的显微组织演变及力学性能

史蒲英[1,2]，刘向宏[2]，任 勇[2]，田 增[3]，张丰收[2]，何卫锋[1]

1. 西安交通大学 机械工程学院 航空发动机研究所，西安 710049；
2. 西部超导材料科技股份有限公司，西安 710018；
3. 空军工程大学 航空工程学院，西安 710038

摘 要：研究激光冲击强化(LSP)对 Ti6242 合金显微组织演变和力学性能的影响，包括残余应力、表面粗糙度、维氏显微硬度、拉伸力学性能和高周疲劳性能。结果表明，LSP 使样品表面和近表面产生残余压应力，表面残余压应力最大值达到−661 MPa，其影响深度大于 1000 μm，且残余压应力随深度增加而减小，但最大残余压应力值并非出现在样品表面。Ti6242 合金的表面粗糙度和维氏显微硬度均随着冲击次数的增加而增加。3 次激光冲击强化后，合金表面硬化层深度达到约 700 μm。激光冲击强化提高了低角度晶界的比例，改变了晶粒的择优取向，同时使近表面 α 相的极密度从 2.41 增加到 3.46。由于加工硬化，LSP 样品的表面硬度随着冲击次数的增加而增加，但 LSP 对拉伸性能的影响很小。与未处理的样品相比，LSP 样品的高周疲劳寿命增加了 20%以上，这是由于 LSP 处理导致的试件表面残余压应力抑制了疲劳裂纹的萌生和扩展。

关键词：双相 Ti6242 合金；表面改性；激光冲击强化；梯度组织；高周疲劳性能

(Edited by Wei-ping CHEN)